HHS Public Access

Author manuscript

Nat Nanotechnol. Author manuscript; available in PMC 2010 December 01.

Published in final edited form as:

Nat Nanotechnol. 2010 June ; 5(6): 412–416. doi:10.1038/nnano.2010.81.

Liquid glass electrodes for nanofluidics

Sanghyun Lee[a],

Department of Mechanical Engineering, POSTECH, Pohang, 790-784, South Korea

Ran An, and

Department of Biomedical Engineering, University of Michigan, Ann Arbor, Michigan 48109, USA

Alan J. Hunt[b]

Department of Biomedical Engineering, Center for Ultrafast Optical Science, University of Michigan, Ann Arbor, Michigan 48109, USA

Abstract

Nanofluidic devices exploit molecular-level forces and phenomena to increase their density, speed and accuracy1. However, fabrication is challenging because dissimilar materials need to be integrated in three dimensions with nanoscale precision. Here we report a three-dimensional nanoscale liquid glass electrode (NLGE) made from monolithic substrates without conductive materials by femtosecond laser nanomachining. The electrode consists of a nanochannel terminating at a nanoscale glass tip that becomes a conductor in the presence of high electric fields through dielectric breakdown, and returns to an insulator when this field is removed. This reversibility relies on control of nanoampere breakdown currents and extremely fast heat dissipation at nanoscale volumes. We use the NLGE to fabricate a nano-injector that includes an electrokinetic pump, 4 μm across with 0.6 μm channels, and capable of well-controlled flow rates below 1 fL/s. The electrode can be easily integrated into other nanodevices and fluidic systems, including actuators and sensors.

Since the earliest work in nanofluidics working with nanopores in lipid bilayers2, novel nanofabrication techniques have been developed to place artificial nanochannels and nanopores in hard and soft materials by electron-beam lithography3, nanoscale-depth photolithography4–6, sacrificial layer deposition7, and track-etching polymer membranes8. Although these advances in nanofabrication have placed fabrication of nanoscale devices

[b]To whom correspondence should be addressed; Tel: 734-615-0331, Fax: 734-936-2116, ajhunt@umich.edu.
[a]toshlee@umich.edu

Author contributions

S.L. discovered the phenomena and the governing mechanism. S.L. conceived and designed the experiments. S.L. performed all the experiments except the I-V measurements in fused silica substrates, which were done by R.A. S.L. performed the numerical simulation and analyzed the simulation results. S.L. developed the nano-injector and analyzed the performance. S.L. and A.J.H. developed the breakdown model, discussed the results, and co-wrote the paper. A.J.H. guided the overall thrust and direction of this research.

Additional information

Supplementary information accompanies this paper at www.nature.com/naturenanotechnology.

within reach, they are poorly suited to producing diverse 3D geometries more complicated than in-plane nanochannels or nanopores. As a non-contacting 3D nanofabrication tool, fs-laser nanomachining can produce true 3D geometries and fluidic conduits, as the laser focus freely moves inside transparent substrates such as glass and PDMS to create channels with diameters typically 500–600 nm, and as small as 100 nm9–13. In addition, post-processing by fs-laser nanomachining enables straightforward integration of 3D nanofluidic components into existing microfluidic devices.

As the scale of fluidic systems is miniaturized, integrating multiple processing steps becomes increasingly difficult, especially incorporation of materials of different electrical, mechanical, chemical, or optical properties. Fabrication of fluidic actuators and sensors such as micropumps14–16 and electrochemical detectors17–21 is complicated by complex structures such as mechanical moving parts, and the requirement for multiple materials. Purely electrical components such as electrokinetic actuators and sensors are preferable because of the proven advantages in avoiding mechanical moving parts and producing plug-like fluid flows with minimal shear and mixing22. For these electrical devices to achieve their full potential, however, the integration of conducting and non-conducting materials into a single device is essential. This has been approached using lithography-based multilayer processes, and protocols have been introduced to incorporate conducting materials into dielectric substrates17.

Nevertheless, configuring 3D nanoscale electrodes in nanodevices is challenged by the requirement for nanoscale precision over the entire multi-layering process. To eliminate the incorporation of conductive materials and enable monolithic device configurations, we examine application of high field phenomena to enable current conduction by dielectric breakdown, which can be induced at the nanoscale even under mild potentials (~several volts). Although the high field currents accompanying dielectric breakdown are usually problematic due to excess heat generation and thermal damage, we find that at the nanoscale high fields can induce reversible and damage-free dielectric breakdown owing to the extremely fast dissipation of heat from nanoscale volumes. This allows dielectric materials such as glass to serve as conductors, eliminating the need to incorporate metal electrodes.

Based on these findings we introduce the NLGE to power fluidic devices, allowing 3D electrodes to be configured in monolithic dielectric substrates. NLGEs are fabricated by fs-laser nanomachining, and are composed of an electrolyte-filled nanochannel “wire” with a nanoscale glass wall electrode at the tip (Fig. 1a). Even mild potentials of several volts produce extreme fields of the order of mega volts per meter across the glass wall, producing dielectric breakdown that allows current flows. The stable, controllable, and reproducible behaviors of the NLGE arise from two fundamental phenomena: 1) the nanochannel wire that guides the electric currents to the NLGE tip limits the breakdown current to the order of nanoamperes by imposing a high in-series resistance (Supplementary 1), and 2) nanoscale confinement of the current conduction protects the NLGE tip from the thermal damage by enabling extremely fast heat dissipation.

The fundamental electrical characteristics were studied using a simple configuration (Fig. 1a), wherein two NLGEs share a single dielectric tip. On one side the electrolytic fluid is

supplemented with fluorescent rhodamine110 (R110, 40μM) molecules to detect if fluids cross the NLGE tip when it conducts currents. With 10V constant potential applied, an abrupt onset of current conduction is observed as the thickness of the tip is reduced by 10 nm increments (Fig. 1 and ref. 12 for the nanomachining setup). When the wall is thinned to 180±70 nm (Fig. 1a and Supplementary 2), currents abruptly start to flow (~18.4 nA) through the tip, without permanent alteration of electrical properties, or apparent structural and material damage. While current densities are as high as 7×10^4 [A/m^2], no fluorescence is observed in the downstream channel (Fig. 1b), showing that no bulk fluid flows cross the NLGE tip. This indicates that the thin nanoscale glass wall works as a conductor allowing electrical currents, but blocking fluid flows despite electroosmotic pressures of about 6 kPa (Supplementary 3.2) on the NLGE tip. After further machining to remove the wall (Fig. 1c), the current increases 3-fold to 53.4 nA, and as expected electroosmotic flow (EOF) drives fluorescent fluids through the now continuous channel (Fig. 1d).

What mechanism underlies the reversible transition of the glass wall from dielectric to conductor? Potentially nanopores could form at the NLGE tip, allowing current conduction while excluding the fluorescent molecules. However, we conclude that nanopores do not contribute to the current conduction of the NLGE. For pores larger than R110 molecules, a possible R110 exclusion mechanism is the permselectivity, but this is unlikely since R110 is nearly neutral at pH of 7 and the electrical double layers (EDL) in the 100 mM buffer solution are only about 1nm thick23. Alternatively nanopores smaller than R110 molecules could carry ionic flows across the NLGE tip. However, for such a small pore anomalous fluorescence distribution is expected near the tip as the fluorophore is enriched and ions depleted due to the EDL overlap inside the nanopores4–6, 24–25; this is not observed. In addition, the steep and abrupt current transitions of the NLGE (Fig. 1e, f, and g) are inconsistent with the I-V characteristics of nanopores, which show gradually increasing current4. Instead, the I-V characteristics of the NLGE are similar to those of Zener diodes.

We conclude that the high field current conduction depends on reversible dielectric breakdown. Other potential high field mechanisms include tunneling and migration of ionic impurities, but these do not fully explain the anomalous electrical characteristics of the NLGE. First, tunneling is easily excluded since the NLGE tip is too thick (~200nm) for tunneling to support significant current density; silicon dioxide (SiO_2) layers must be thinner than 3 nm to produce significant tunneling currents in CMOS semiconductors26. Ionic impurities contained in glass such as Na^+ may modulate the characteristics of the NLGE, but they are not required for conduction since similar I-V behavior is observed for NLGEs in fused silica, where impurities are negligible (Fig. 1e and g). Furthermore, even in glass, current-carrying ionic impurities in the NLGE tip would deplete in about a millisecond (Supplementary 4), so we conclude that current flow across the glass wall does not fundamentally depend on ionic impurities, though they may modulate the breakdown threshold (e.g. compare Fig. 1e and g). However, reversible dielectric breakdown is surprising and unusual, so the mechanism warrants further consideration.

Dielectric breakdown of thin insulating SiO_2 layers in semiconductors has been the subject of intensive research predominantly aimed at preventing device failures. The abruptly increased conductivity accompanying dielectric breakdown results in substantial power

dissipation, and the resultant heating causes irreversible damage to the device. However, the irreversible characteristics of the dielectric breakdown are not necessarily intrinsic, and can be avoided if the currents are well-controlled27. In the NLGE, current control is achieved by the mega-ohm resistance of the nanochannel, which provides a series resistance that limits currents across the tip to the order of nanoamperes. Nevertheless, considering the substantial current density at the tip, as high as several mega amperes per unit area, it is still surprising that thermal damage is avoided. This critically depends on nanoscale confinement: for breakdown occurring in the nanoscale glass tip, the surface area to volume ratio is extraordinarily large, allowing extremely fast heat dissipation that prevents thermal damage.

Numerical analyses reveal that the nanoscale spherical tip does not experience significantly increased temperatures despite resistive heat generation reaching mega watts/cm^3. Based on measurements of the electrical behavior of the NLGE before and after removing the tip, the detailed electrical properties of the NLGE can be calculated (Table I and Supplementary 3.1). These experimental data allow numerical analyses of the electrical and the thermal properties of the NLGE, taking into account the three-dimensional shape of the NLGE tip (Supplementary 5). For numerical simulations of the breakdown phenomena at the NLGE tip, the conductivity transition of the tip was modeled as $\sigma(E)=\sigma_o/(1-E/E_{bk})^n$, based on the M-factor ($=1/(1-|V/V_{bk}|^n)$, $3 \leq n \leq 6$), which is commonly used to describe Zener breakdown (Supplementary 5.2); σ_o: low field conductivity of glass ($\approx 10^{-14}$ [S/m], ref. 28), n: exponent describing the nonlinear onset of breakdown, E: electric field strength [V/m], and E_{bk}: electric field strength at breakdown [V/m]. The specific value of E_{bk} of 37.5MV/m can be explicitly determined from the experiments, and an exponent n = 6 gives the best agreement between the experimental and the numerical I-V graphs (Fig. 1g and Supplementary 5.3).

The potential drop across the tip during breakdown is nearly constant as the applied potential increases (Fig. 2a: marked with the dot-line circle), resulting in the electric field flattening at the center of the tip. This occurs because very small increases in the electric field strength can induce sharp increases of the conductivity; this is similar to the non-linear behavior that results in nearly constant voltages across Zener diodes. The concave NLGE tip is structurally thinnest at the center, where the electric field strength is maximal, and becomes thicker in the radial direction. Consequently breakdown and conduction do not occur evenly over the entire area of the tip, but starts from the center and expands radially outward with increasing voltage (Fig. 2b, Supplementary 5.5). Because the breakdown occurs within nanoscale dimensions, the large surface area to volume ratio of the nanoscale volume undergoing breakdown allows extremely fast heat dissipation and surprisingly small temperature rises (Fig. 2e), avoiding thermal damage despite the extremely high energy density of Joule heating (Fig. 2c and d). Significant temperature rises calculated for bigger tips indicate that even micron scale tips would sustain thermal damage (Fig. 2f). Thus, reversible dielectric breakdown is a fundamentally nanoscale phenomenon.

As an example application, we applied a NLGE to construct a nano-injector, driven by a submicron cross-section electrokinetic (EK) pump29. Although smaller pumps exist in nature (e.g. ion pumps), to the best of our knowledge this is the smallest pump of any kind ever fabricated and integrated in a microchip de novo; the size of the EK pump is similar to a human red blood cell (Fig. 3a). This actuator is also remarkable in its construction from a

monolithic substrate, circumventing fabrication difficulties related to the incorporation of conductive materials for the nanoscale electrodes. When an electric potential is applied between E_1 and E_2 (Fig. 3a and b), the electric current induces EOF with pressure driven back flows along the three perpendicular nanochannels. The nanochannel bundle comprising the NLGE-driven EK pump body is equivalent to the porous membrane in conventional EK pumps29. The pressure drives hydrodynamic flows out of the single horizontal nanochannel, the fluid exit (Fig. 3c), where test specimens such as cells can be placed. The pumping characteristics were assessed based on the test operations with 14 and 38 V potentials (TABLE II) and the performances with 380V potential and trimethylammoniopropane sulfonate (TMAPS) additives for improving efficiencies were extrapolated based on the conventional EK pump analysis procedures29. Although a pumping mechanism is required for many microfluidic systems, the difficulty of implementing electrodes and porous membranes within micron scale footprints poses serious challenges. The NLGE-based EK pump can drive sufficient flows for nanoscale actuators, and demonstrates simple and straightforward integration of the 3D nanoscale electrode into a nanodevice.

In summary, the remarkable ability to produce well-stabilized reversible dielectric breakdown across a nanoscale thin dielectric wall enables construction of a novel form of electrode, the NLGE, which has distinct advantages over conventional electrodes. NLGEs are well suited to nanoscale implementation of electrodes into complex 3D lab-on-a-chip devices, enabling straightforward integration of nanoscale actuators and sensors within fluidic systems. NLGEs produced by 3D fs-laser nanomachining can be directly inscribed in three-dimensions in monolithic transparent substrates to interface with existing micro/nanofluidic channels, thereby eliminating complicated multi-layer processing. As a demonstration, we constructed a nano-injector driven by an extraordinarily small EK pump, fabricated in a monolithic glass substrate using a single machining process. In principal, NLGEs can be applied to virtually any transparent platform, with unprecedented freedom to configure micro/nanofluidics for improved device densities and functionality, thus introducing a new design and fabrication paradigm to micro/nanofluidics.

Supplementary Material

Refer to Web version on PubMed Central for supplementary material.

Acknowledgements

We are grateful to Steven Yalisove and Kwan Hyoung Kang for useful discussions. We thank Intralase corp. for the laser. This work was supported by NIH R21 EB006098.

References

1. Schoch RB, Han J, Renaud P. Transport phenomena in nanofluidics. Rev. Mod., Phys. 2008; 80:839–883.
2. Bayley H, Cremer PS. Stochastic sensors inspired by biology. Nature. 2001; 413:226–230. [PubMed: 11557992]
3. Saleh OA, Sohn LL. Quantitative sensing of nanoscale colloids using a microchip Coulter counter. Rev. Sci. Instrum. 2001; 72:4449–4451.

4. Chang H-C, Yossifon G. Understanding electrokinetics at the nanoscale: a perspective. Biomicrofluidics. 2009; 3:012001.

5. Fu J, Schoch RB, Stevens AL, Tannenbaum SR, Han J. A patterned anisotropic nanofluidic sieving structure for continuous-flow separation of DNA and proteins. Nature Nanotechnology. 2007; 2:121–128.

6. Wang Y, Stevens AL, Han J. Million-fold Preconcentration of Proteins and Peptides by Nanofluidic Filter. Anal. Chem. 2005; 77:4293–4299. [PubMed: 16013838]

7. Karnik R, Castelino K, Fan R, Yang P, Majumdar A. Effects of Biological Reactions and Modifications on Conductance of Nanofluidic Channels. Nano Lett. 2005; 5:1638–1642. [PubMed: 16159198]

8. Zhou K, Kovarik ML, Jacobson SC. Surface-Charge Induced Ion Depletion and Sample Stacking near Single Nanopores in Microfluidic Devices. J. Am. Chem. Soc. 2008; 130:8614–8616. [PubMed: 18549214]

9. Joglekar AP, Liu H, Meyhöfer E, Mourou G, Hunt AJ. Optics at critical intensity: applications to nanomorphing. Proc. Nat. Acad. Sci. USA. 2004; 101:5856–5861. [PubMed: 15071188]

10. Kim TN, Campbell K, Groisman A, Kleinfeld D, Schaffer CB. Femtosecond laser-drilled capillary integrated into a microfluidic device. Appl. Phys. Lett. 2005; 86:201106.

11. Mcdonald JP, Mistry VR, Ray KE, Yalisove SM. Femtosecond pulsed laser direct write production of nano- and microfluidic channels. Appl. Phys. Lett. 2006; 88:183113.

12. Ke K, Hasselbrink EF, Hunt AJ. Rapidly prototyped three-dimensional nanofluidic channel networks in glass substrates. Anal. Chem. 2005; 77:5083–5088. [PubMed: 16097742]

13. Lee S, Bull JL, Hunt AJ. Acoustic limitations on the efficiency of machining by femtosecond laser-induced optical breakdown. Appl. Phys. Lett. 2007; 91:023111.

14. Harrison DJ, Manz A, Fan ZH, Ludi H, Widmer HM. Capillary Electrophoresis and Sample Injection Systems Integrated on a Planar Glass Chip. Anal. Chem. 1992; 64:1926–1932.

15. Takamura Y, et al. Low-voltage electroosmosis pump for stand-alone microfluidics devices. Electrophoresis. 2003; 24:185–192. [PubMed: 12652590]

16. Hong CC, et al. A functional on-chip pressure generator using solid chemical propellant for disposable labon-a-chip. Lab Chip. 2003; 3:281–286. [PubMed: 15007459]

17. Baldock SJ, Fielden PR, Goddard NJ, Prest JE, Treves Brown BJ. Integrated moulded polymer electrodes for performing conductivity detection on isotachophoresis microdevices. Chromatogr. A. 2003; 990:11–22.

18. Hebert NE, Snyder B, McCreery RL, Kuhr WG, Brazill SA. Performance of Pyrolyzed Photoresist Carbon Films in a Microchip Capillary Electrophoresis Device with Sinusoidal Voltammetric Detection. Anal. Chem. 2003; 75:4265–4271. [PubMed: 14632145]

19. Wu CC, Wu RG, Huang JG, Lin YC, Chang H-C. Three-Electrode Electrochemical Detector and Platinum Film Decoupler Integrated with a Capillary Electrophoresis Microchip for Amperometric Detection. Anal. Chem. 2003; 75:947–952. [PubMed: 12622389]

20. Baldwin RP, et al. Fully Integrated On-Chip Electrochemical Detection for Capillary Electrophoresis in a Microfabricated Device. Anal. Chem. 2002; 74:3690–3697. [PubMed: 12175155]

21. Laugere F, et al. On-Chip Contactless Four-Electrode Conductivity Detection for Capillary Electrophoresis Devices. Anal. Chem. 2003; 75:306–312. [PubMed: 12553766]

22. Paul PH, Garguilo MG, Rakestraw DJ. Imaging of pressure- and electrokinetically driven flows through open capillaries. Anal. Chem. 1998; 70:2459–2467. [PubMed: 21644766]

23. Probstein, RF. Physicochemical hydrodynamics. 2nd edition. Wiley-Interscience; 2003. ISBN 0-471-45830-9

24. Pu Q, Yun J, Temkin H, Liu S. Ion-Enrichment and Ion-Depletion Effect of Nanochannel Structures. Nano Lett. 2004; 4(6):1099–1103.

25. Eijkel JCT, Van den Berg A. Nanofluidics: what is it and what can we expect from it. Microfl. nanofl. 2005; 1:249–267.

26. Chau RS. Intel's Breakthrough in High-K Gate Dielectric Drives Moore's Law Well into the Future. Technology@Intel Magazine. 2004:1–7.

27. Sune J, Nafria M, Aymerich X. Reversible dielectric breakdown of thin gate oxides in mos devices. Microelectron. Reliab. 1993; 33:1031–1039.

28. Gamow, G. Matter, Earth & Sky. Revised edition. New York: Prentice-Hall; 1965.

29. Reichmuth DS, Chirica GS, Kirby BJ. Increasing the performance of high-pressure, high-efficiency electrokinetic micropumps using zwitterionic solute additives. Sens. and Act. B. 2003; 92:37–43.

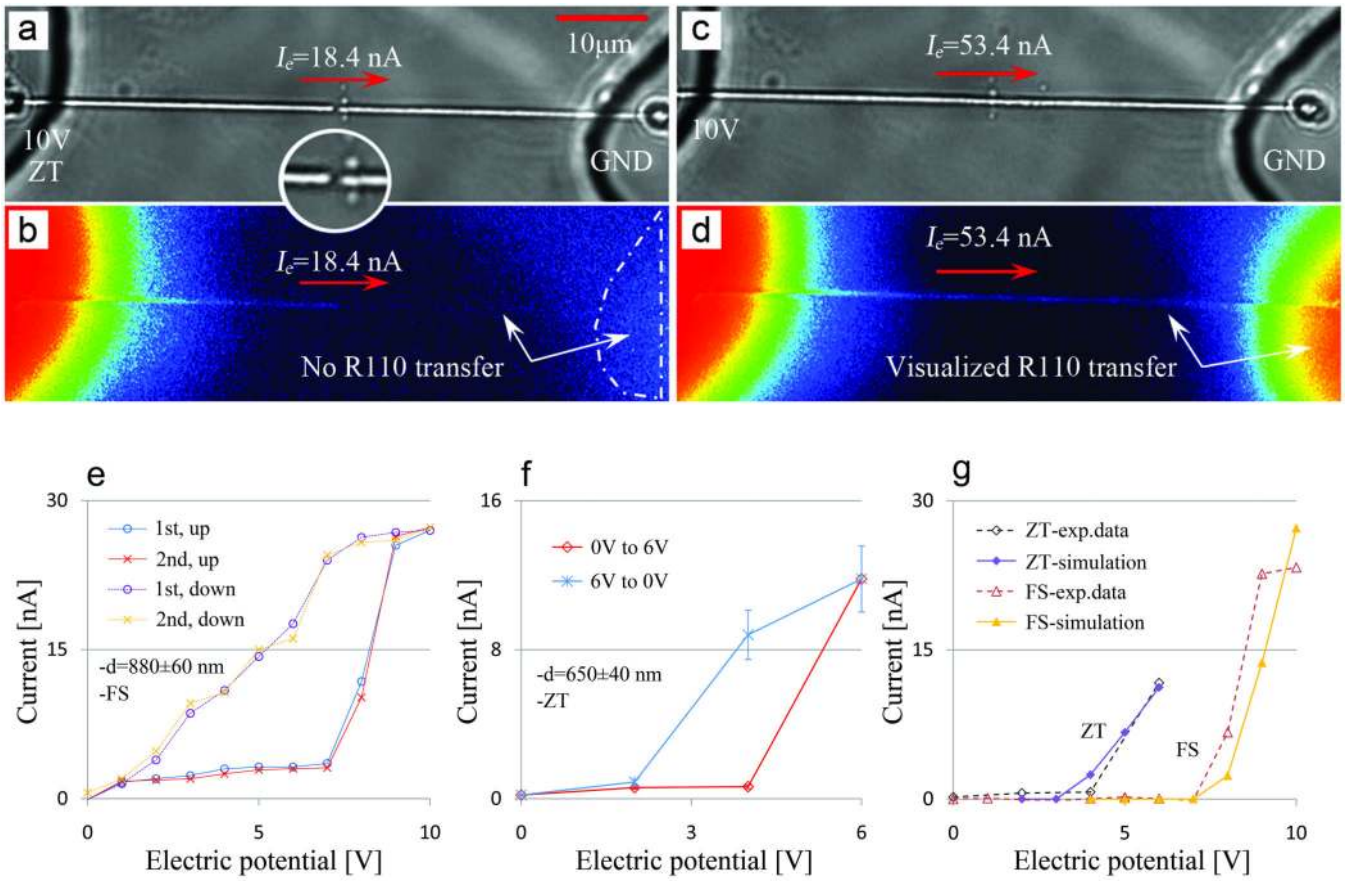

Figure 1. Reversible dielectric breakdown across a thin glass wall separating two channels (i.e. a NLGE)

Electric currents are measured simultaneously with fluorescent visualization using rhodamine110 (R110, 40 μM) diluted in the phosphate buffer (100mM, pH=7.0). **a–d**, Light and fluorescence micrographs of NLGE in zinc-titancia glass (ZT, Corning 0211). **a**, Light micrograph of the NLGE carrying a current of 18.4 nA with 10 V potential (thickness of tip=180±70 nm, see supplemental 2). **b**, Despite current flow, the NLGE tip blocks direct fluid transfer, as evidenced by lack of fluorescence in the right reservoir (pseudo-color conversion of grey-scale to black-blue-green-yellow-red format, after 4 images were averaged for noise reduction). **c**, Elimination of the NLGE tip increases the electric current to 53.4 nA. **d**, After the tip is eliminated, direct transfer of R110 is seen (the same pseudo-color conversion as **b**, after 8 images were averaged for noise reduction). **e**, An abrupt current jump due to dielectric breakdown exhibits hysteresis when the voltage is cycled in a fused silica (FS) substrate (two cycles of many similar cycles are shown). **f**, A similar breakdown current jump and hysteresis occurs with a zinc-titania substrate. Error bars indicate current fluctuations. **g**, Simulated and measured I-V data for rising potential in zinc-titania and fused silica substrates.

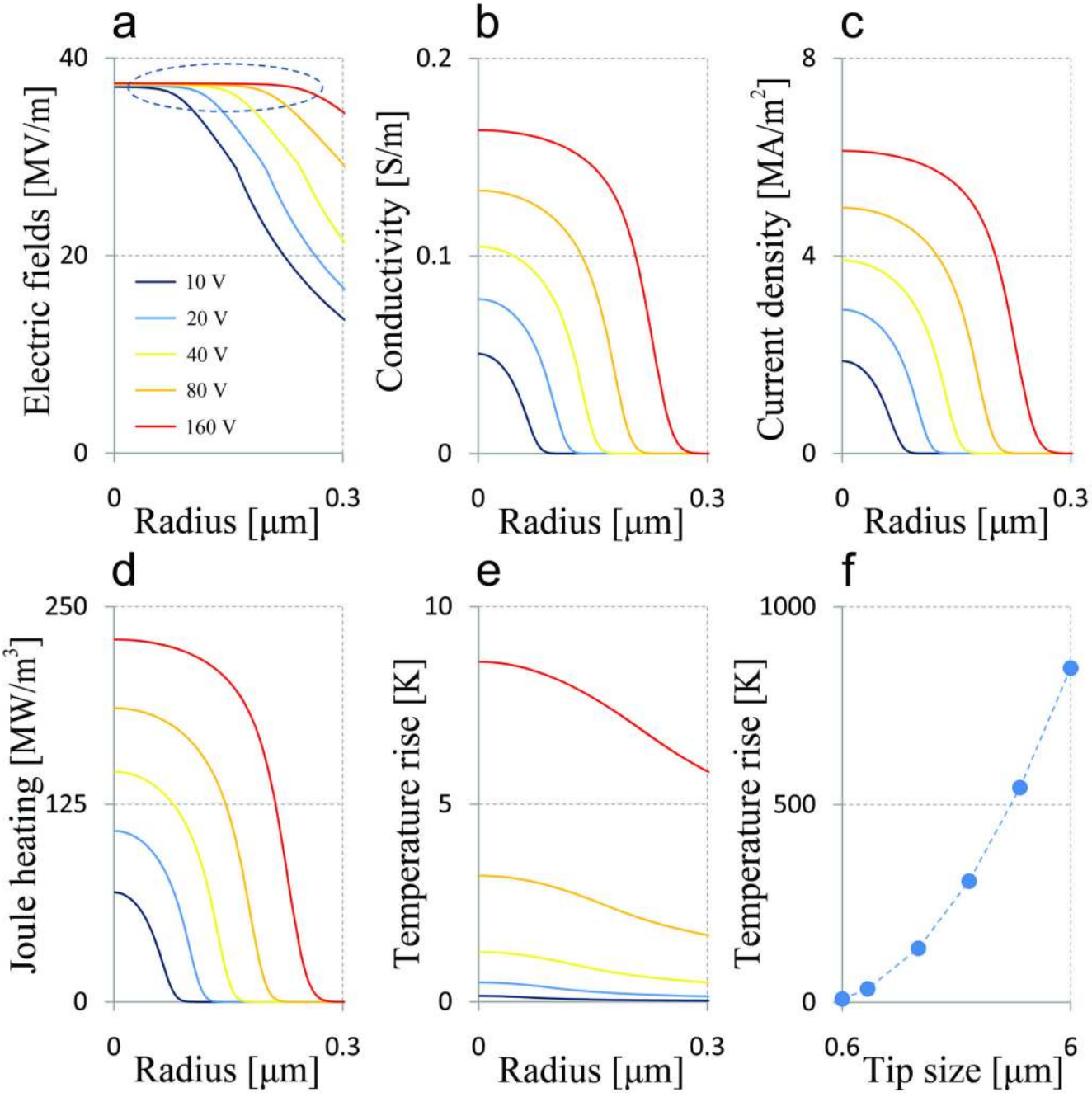

Figure 2. Simulation results with electric potentials from 10V to 160V

Radial distance is from the center of the NLGE tip. **a**, The electric field distribution at the tip shows peak flattening. Voltages correspond to the same colors in all panels **b**, The conductivity distribution at the tip shows nanoscale confinement of the breakdown. **c**, The current density at the tip is as high as several mega-amperes/m^2. **d**, At the nanoscale tip, Joule heating of the order of mega-watts/cm^3 is generated by the high current density. **e**, Increases in the steady state temperature at the NLGE tip are surprisingly small due to extremely rapid heat dissipation from nanoscale volumes. **f**, Simulations reveal that even

micron scale tips would encounter large temperature rises causing irreversible thermal damage.

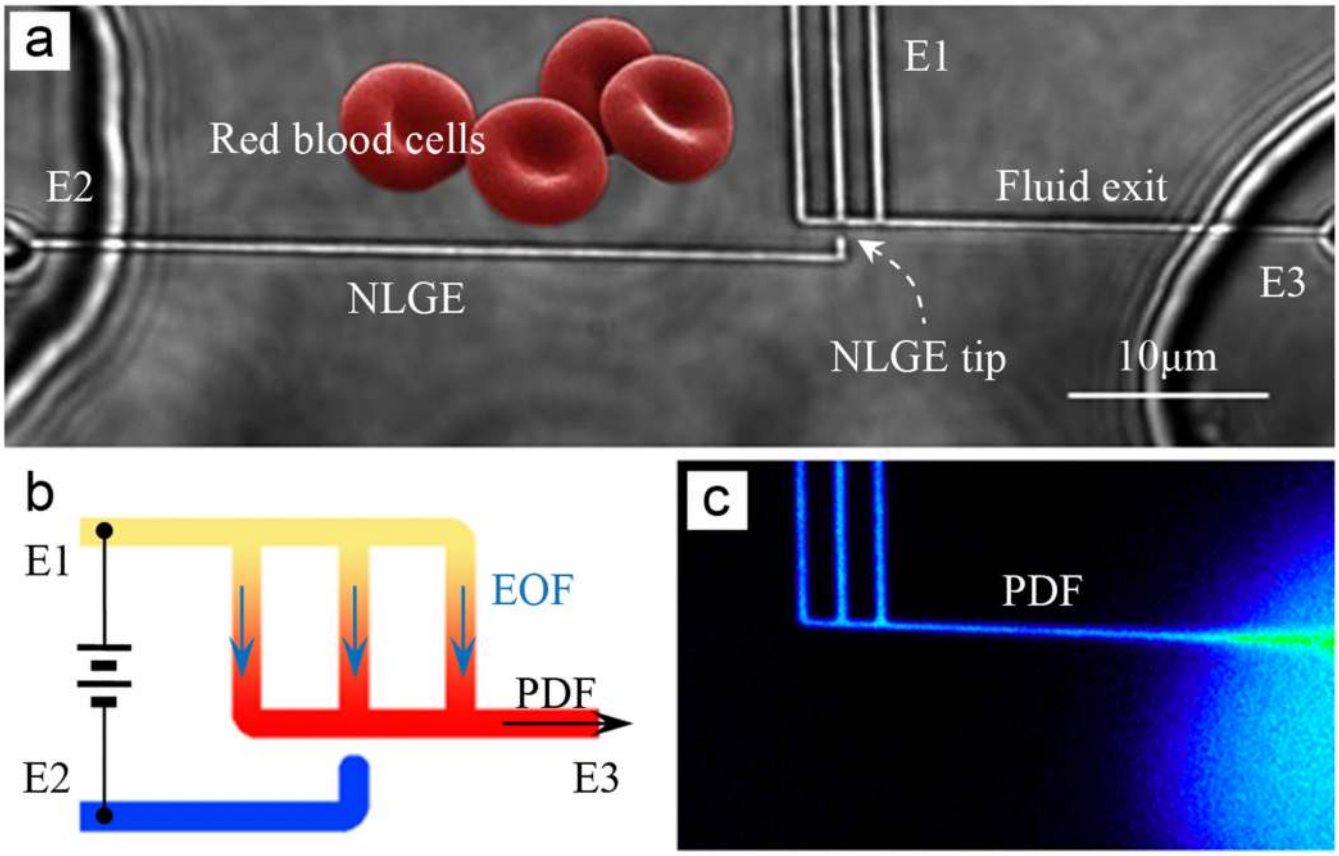

Figure 3. A prototype nano-injector driven by a single NLGE EK pump

a, Bright field micrograph of the NLGE-based nano-injector; superimposed images of red blood cells are for the size comparison. **b**, A schematic of the NLGE driven EK pump (yellow to red represents low to high pressure). **c**, Fluorescently visualized pressure driven fluid injection with 14V potential between E1 and E2 as shown in **b**.

TABLE I

Electrical properties of the NLGE and the substrate.

	Initial glass wall	Conductive NLGE tip	Nanochannel
Thickness[m]	$1000\pm50\times10^{-9}$	$180\pm50\times10^{-9}$	
Potential [V]	10	6.5 (turn-on)	3.5
Conductivity [S/m]	$\sim10^{-14}$	$\sim0.05^{\dagger}$	1.01
Resistance [Ω]	$\sim10^{12}$	356×10^{6}	187×10^{6}

†This is the averaged conductivity of the NLGE tip, which varies according to the radial position (see Supplementary 5.3). The low field conductivity of glass is from ref. 28.

TABLE II

Performance estimates for the nano-injector.

V_{cc} [V]	I [μA]	P_{total} [μW]	Q_{inj} [fL/s]	ΔP_{inj} [kPa]	η [%]	Additive (2.2M TMAPS) ΔP_{inj} [kPa]	Q_{inj} [fL/s]	η [%]
14	0.02	0.29	0.38	2.84	0.37×10^{-3}	*15.8*	*2.1*	*0.69*
38	0.145	5.51	2.63	19.8	0.95×10^{-3}	*110.6*	*14.6*	*1.78*
380	*1.92*	*727*	*34.8*	*263*	*1.26×10^{-3}*	*1462*	*194*	*2.35*

V_{CC} is the total applied electrical potential, I is the resulting electrical current, P_{total} is the total power consumption, Q_{inj} is the injection flow rate at the exit nozzle (fL/s=10^{-15} liters per second), P_{inj} is the pressure drop at the injection, and η is the efficiency of the hydrodynamic flow injection versus the electrical power consumption. The data in italics are theoretical extrapolations based on the linear scaling assumption. The pumping performances are estimated using established approaches for pump analyses29.